Electrochimica Acta 434 (2022) 141300

Contents lists available at ScienceDirect

Electrochimica Acta

journal homepage: www.journals.elsevier.com/electrochimica-acta

Linear correlation between state-of-health and incremental state-of-charge in Li-ion batteries and its application to SoH evaluation

Jici Wen [a,c], Qingrong Zou [b], Chunguang Chen [a,c,*], Yujie Wei [a,c,*]

[a] State Key Laboratory of Nonlinear Mechanics (LNM), Institute of Mechanics, Chinese Academy of Sciences, Beijing 100190, China
[b] School of Applied Science, Beijing Information Science and Technology University, Beijing 100192, China
[c] School of Engineering Sciences, University of Chinese Academy of Sciences, Beijing 100049, China

ARTICLE INFO

Keywords:
State-of-health evaluation
State-of-charge
Lithium-ion battery
Incremental capacity curve
Sliding voltage window

ABSTRACT

SoH (State-of-Health) evaluation is of pressing need in the health management of commercial Li-ion batteries and has been a topic of intensive research. A simple route to supply a quick, non-destructive, and preferably on-site assessment of SoH with high fidelity is desired. In this paper, analysis based on a partial (dis)charge and a sliding voltage window on the constant-current (dis)charge voltage-time curve may fulfill the need. The incremental State-of-Charge (ΔS_{oC}) (derived from the sliding window) is proportional to the SoH within a suitable voltage region. The slope k of the $S_{oH} - \Delta S_{oC}$ curve and its extrapolated interception at SoH=1, denoted as ΔS^1_{oC}, can then be used to differentiate the remaining life of batteries of the same SoH. The proposed SoH evaluation method, along with the linearity characterized by k and ΔS^1_{oC}, make it an appealing route toward quick and on-site health management of batteries.

1. Introduction

Li-ion batteries (LIBs) have been extensively used as energy storage systems for portable electronics, electric vehicles, and other fields [1–3]. Immediately after production, LIBs are bound to irreversible degradation, no matter in storage, transportation, in use or lay aside. Quantifying the state of degradation in LIBs is therefore a crucial demand for the economical and reliable operations of LIBs-powered systems [4–8]. The SoH (State-of-Health) is a key parameter evaluating the current working conditions of LIBs. For its self-evident importance, various methods have been proposed to characterize the SoH of LIBs [9–11]. The capacity-fade indicator S_{oH}, defined as the ratio of the current maximum available capacity Q_c to the rated capacity Q_r [11], i.e., $S_{oH} = \frac{Q_c}{Q_r}$, is of general acceptance in the LIBs industry. In fact, in contrast to the simple definition, characterizing the contribution of a particular one out of many mechanisms to the degradation of LIBs (hence SoH) is not an easy job, since the degradation of LIBs often involves multiple interweaving mechanisms and processes [12–17], e.g. active material shedding, loss of electrical contact, lithium loss caused by SEI (Solid--Electrolyte-Interphase) formation, and *etc*. The strong electro-chemo-mechanical coupling behavior during battery degradation [18–22] perplexes the determination of SoH in engineering applications.

Among different technologies to characterize SoH of LIBs [23–26], two strategies have been prevailing, including a direct measurement and an indirect method [27]. With respect to the direct method, the available capacity and internal resistance are the two critical parameters for battery SoH estimation. The ampere-hour counting method is commonly used to measure available capacity through complete charging and discharging batteries at low current rates [28], which is time-consuming for on-site SoH evaluation. The electrochemical impedance spectroscopy technique, through applying a voltage or current excitation to obtain the change of impedance spectrum, may also reflect the battery degradation [29], which is however subject to data noise and constraints in field test.

Methods through indirect analysis are often either physics- or data-driven-based, and the two also include different variants based on the adopted physical model and the strategy applied for feature extraction. Electrochemical-model-based and equivalent-circuit-model-based methods are the two commonly used physics-based approaches. The electrochemical-model-based approach uses a single physical feature involved in the (dis)charge processes, such as Li-ion concentration [30], SEI film thickness [31], and so on, to extract SoH. As the methods involve coupling of multiple fields, one often needs to solve a group of nonlinear partial differential equations [32,33]. The

* Corresponding authors at: State Key Laboratory of Nonlinear Mechanics (LNM), Institute of Mechanics, Chinese Academy of Sciences, Beijing 100190, China.
E-mail addresses: chenchunguang@imech.ac.cn (C. Chen), yujie_wei@lnm.imech.ac.cn (Y. Wei).

https://doi.org/10.1016/j.electacta.2022.141300
Received 15 September 2022; Received in revised form 2 October 2022; Accepted 2 October 2022
Available online 3 October 2022

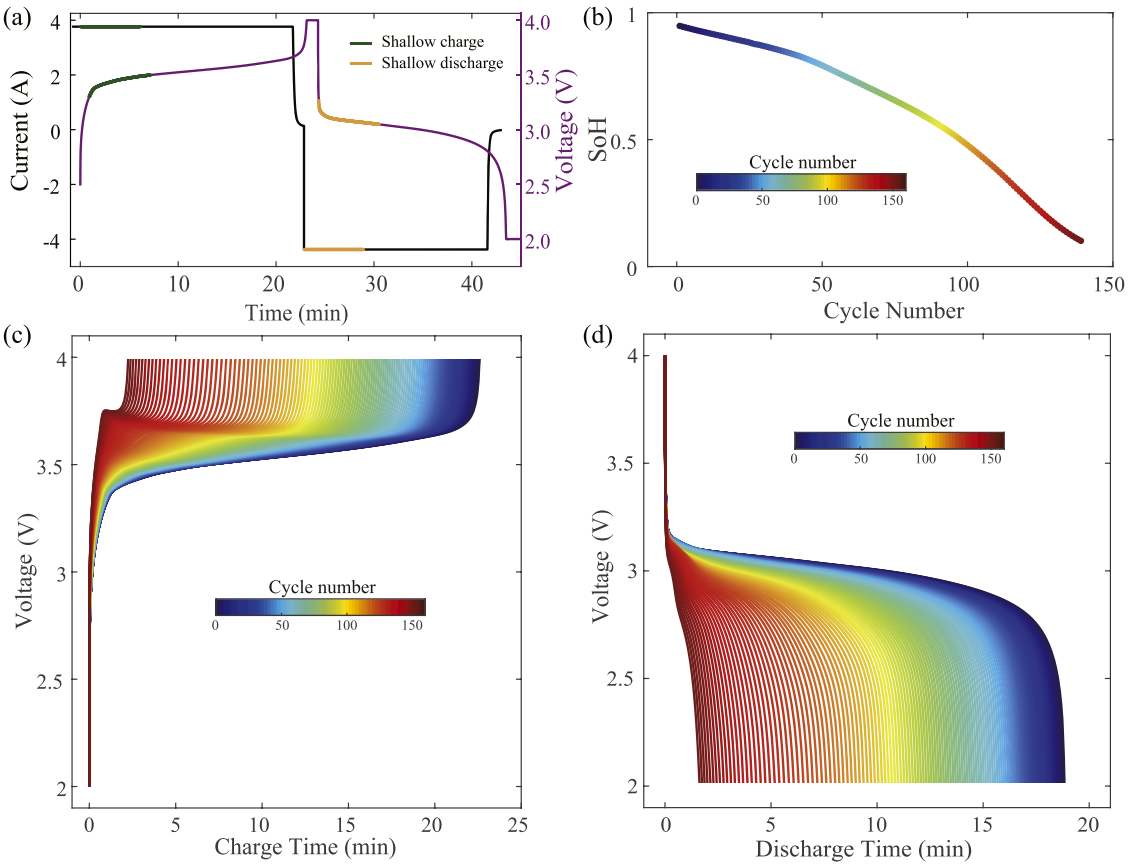

Fig. 1. The evolution of SoH of an LFP/graphite battery. (a) The current-time curve and its corresponding voltage-time response with highlighted shallow CC charge and CC discharge domain in the first full charge-discharge cycle under CC—CV mode (2.5C-3.0D); (b) The SoH vs cycle number curve, in which the color bar denotes cycling history; The voltage-time plots during charging (c) and discharging (d) at different cycles.

equivalent-circuit-model-based methods are of moderate complexity, but limited operating conditions [34].

Data-driven-based methods are sweeping all corners of science, and are also adopted to predict SoH of the energy storage system (such as, battery, supercapacitor, etc.) by extracting essential features from data at hand using either statistical analyses or machine learning techniques [35,36]. Differentiating the contribution of a particular mechanism to capacity degradation and hence to SoH is off the table [37–40]. Both automatic extraction method by deep learning (AEM-DL) framework [41,42] and manual construction based on domain knowledge (MC-DK) framework [43–45] can be utilized for feature extraction. AEM-DL algorithms are usually accompanied with complex computation based on available data, in which the specific meaning of individual features is generally obscure [46,47]. Moreover, the AEM-DL methods use testing data involving a full charging process, from 0% SoC (State-of-Charge) up to 100% SoC at the constant-current constant-voltage (CC—CV) charging mode. To avoid full charging process and reduce the test time, incremental capacity analysis (ICA) methods based on regional capacity and voltage were introduced for SoH estimation [48,49]. However, incremental capacity and differential voltage curves are composed of substantial noise signals and require filtering techniques for data pretreatment. Besides, the ICA method is restricted to low charge current rates (1/5 to 1/25 C-rate) in order to achieve reasonable fidelity for SoH.

Owing to the rapid development of novel data-driven-based methods, many endeavors have been devoted to effective feature extraction for SoH [50–52]. Liu et al. [53,54] estimated SoH with GPR (Gaussian Process Regression) and RVM (Relevance Vector Machine), and such methods can provide the posterior probability of predictions. Li et al. [55] applied transfer learning and network pruning to establish compact convolutional neural network models to improve the accuracy of SoH estimation. Regardless of the tremendous successes, differentiating battery-wise distinctions in SoH using data-driven methods remains challenging. The reliability depends highly on the data characteristics and volume [56]. High computational cost is another issue to prevent its application from on-site application [57].

In this report, we propose a quick, non-destructive, and potentially on-site assessment of SoH with high fidelity, and discuss its implication for differentiating the performance of batteries. We introduce in the second section the data acquisition details, followed with the sliding voltage window strategy to construct the SoH evaluation in Section 3, and report a linear relationship between SoH and the increment SoC. In Section 4 we demonstrate how the slope k of the $S_{oH} - \Delta S_{oC}$ curve and its interception at SoH=1 (ΔS^1_{oC}) can be adopted to make a distinction about the remaining life of the batteries of same SoH. We conclude in Section 5 with further discussions on the implications of the methods for the health management of batteries.

2. Experimental section

The experiments were performed on commercial LFP ($LiFePO_4$)/graphite batteries (LISHEN, 18,650 cylindrical battery, 1.5 Ah nominal capacity). The LFP/graphite batteries were cycled by NEWARE battery testing systems with a sampling frequency of 1 Hz at 25 °C in a temperature-controlled environmental chamber. Typical constant-current constant-voltage (CC—CV) charging and discharging profiles adopted for the cycling measurements are shown in Fig. 1a. The cut-off voltage in constant-current (CC) charging stage and CC discharging stage are set to 4.0 and 2.0 V, respectively. The cut-off current during constant-voltage (CV) stage is set to 0.05C, where 1C is equal to 1.5 A. A dataset including 48 LIBs was generated, including 6 groups and each

Table 1
The charge-discharge settings of the six groups of LIBs. In each group, there are eight batteries which were tested with the same charge and discharge profile listed here.

Group No.	Charge-Discharge Profiles	Abbreviations
1	1.0C charge – 3.0C discharge	1.0C-3.0D
2	1.5C charge – 3.0C discharge	1.5C-3.0D
3	2.0C charge – 3.0C discharge	2.0C-3.0D
4	2.5C charge – 3.0C discharge	2.5C-3.0D
5	2.0C charge – 2.0C discharge	2.0C-3.0D
6	2.5C charge – 2.5C discharge	2.5C-2.5D

applied with the same charge and discharge profile. The 6 charge-discharge profiles are set with different CC (dis)charge rates, what are detailed in Table 1.

With the CC—CV charge and discharge (2.5C-3.0D) applied to an LFP/graphite battery, the current-time curve in the first cycle is what we see in Fig. 1a. With cycling proceeding, the delivered capacity exhibits an apparent decay (see Fig. 1b), suggesting the SoH degradation. Extracting the corresponding voltage-time curves from the charge (Fig. 1c) and discharge (Fig. 1d) at different cycles, it can be seen that the time in the CC charge and CC discharge stages are greatly shortened with cycling, indicating a more prominent voltage-changing (discharging) rate at higher cycle numbers.

3. Modelling

Fig. 1 shows the response of a battery subject to full CC—CV charge and discharge cycle. We are interested in utilizing the voltage change in time during CC charge and CC discharge stages, and proceed to show how we may evaluate SoH from the voltage-time curves during both CC charging and CC discharging processes but with a shallow (dis)charging strategy, as illustrated in Fig. 1a.

3.1. S_{oH}-ΔS_{oC} evolution during discharging

To depict the SoH degradation from the voltage-time curves at CC discharge stages, we examine the variation of time Δt (equivalently ΔS_{oC} through $\Delta S_{oC} = C\Delta t$ where C means (dis)charge rate in the CC stage) for a given voltage drop (ΔV) in the voltage-time curves at different cycles, as illustrated in Fig. 2a. One may think of different ways to determine the starting voltage V_s in a discharge curve. We adopt a correlation analysis based on the spearman coefficient ρ [58] to indicate the statistical dependence of SoH on ΔS_{oC} for a variety of combinations of ΔV

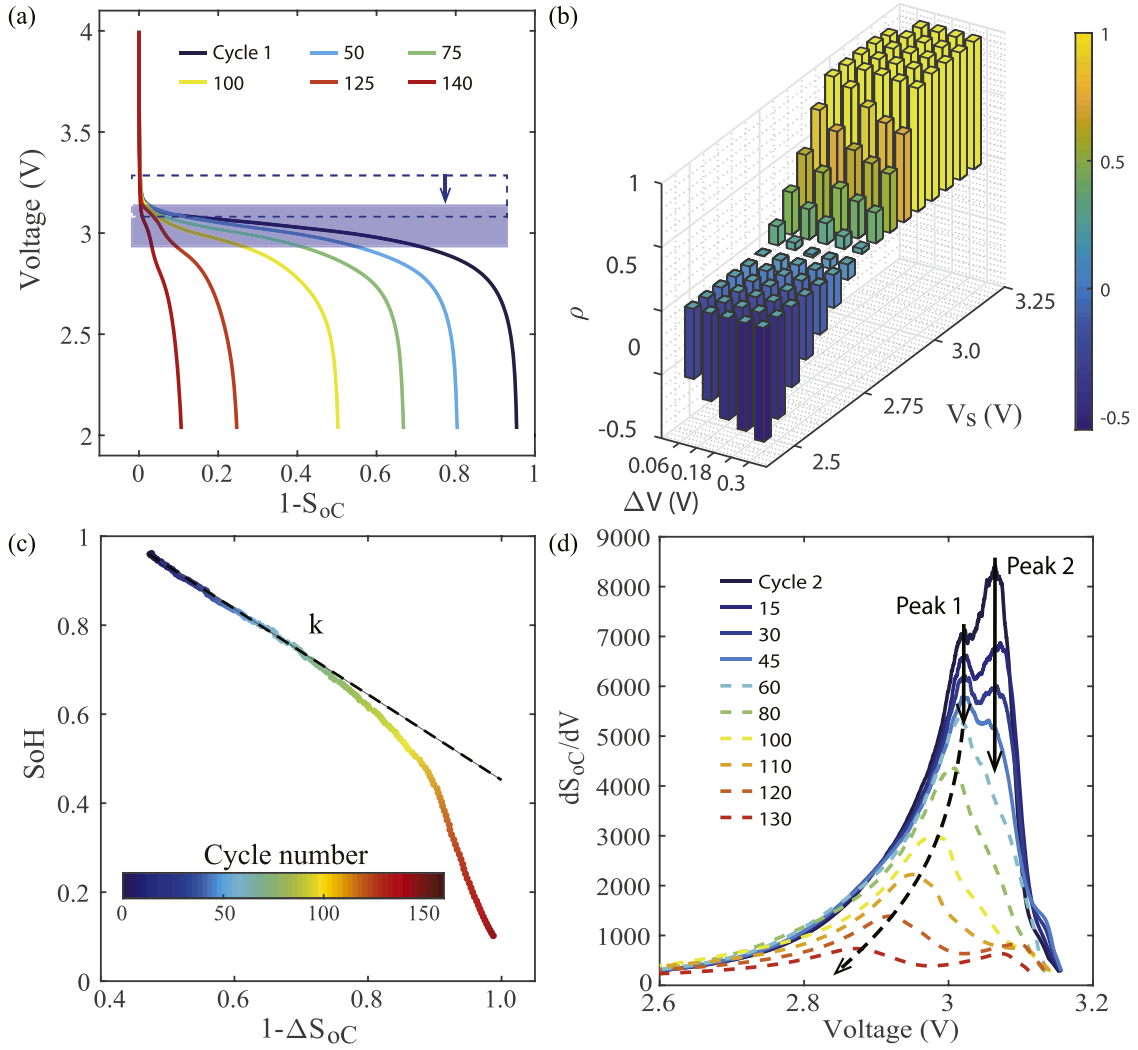

Fig. 2. The S_{oH}-ΔS_{oC} evolution rule during discharging in the total cycle-life of the batteries, cycled with CC—CV mode (2.5C-3.0D). (a) The voltage-(1-S_{oC}) plots during the 3C CC discharge stages at different indicated cycles. The light blue color region marks the selected voltage window for S_{oH}-ΔS_{oC} correlation analysis; (b) The spearman correlation coefficient image between SoH and ΔS_{oC} with different voltage window ($\Delta V, V_s$); (c) The SoH-$(1-\Delta S_{oC})$ plots using the voltage window $\Delta V = 0.3, V_s = 3.3$; (d) The dS_{oC}/dV-voltage curves at different cycles.

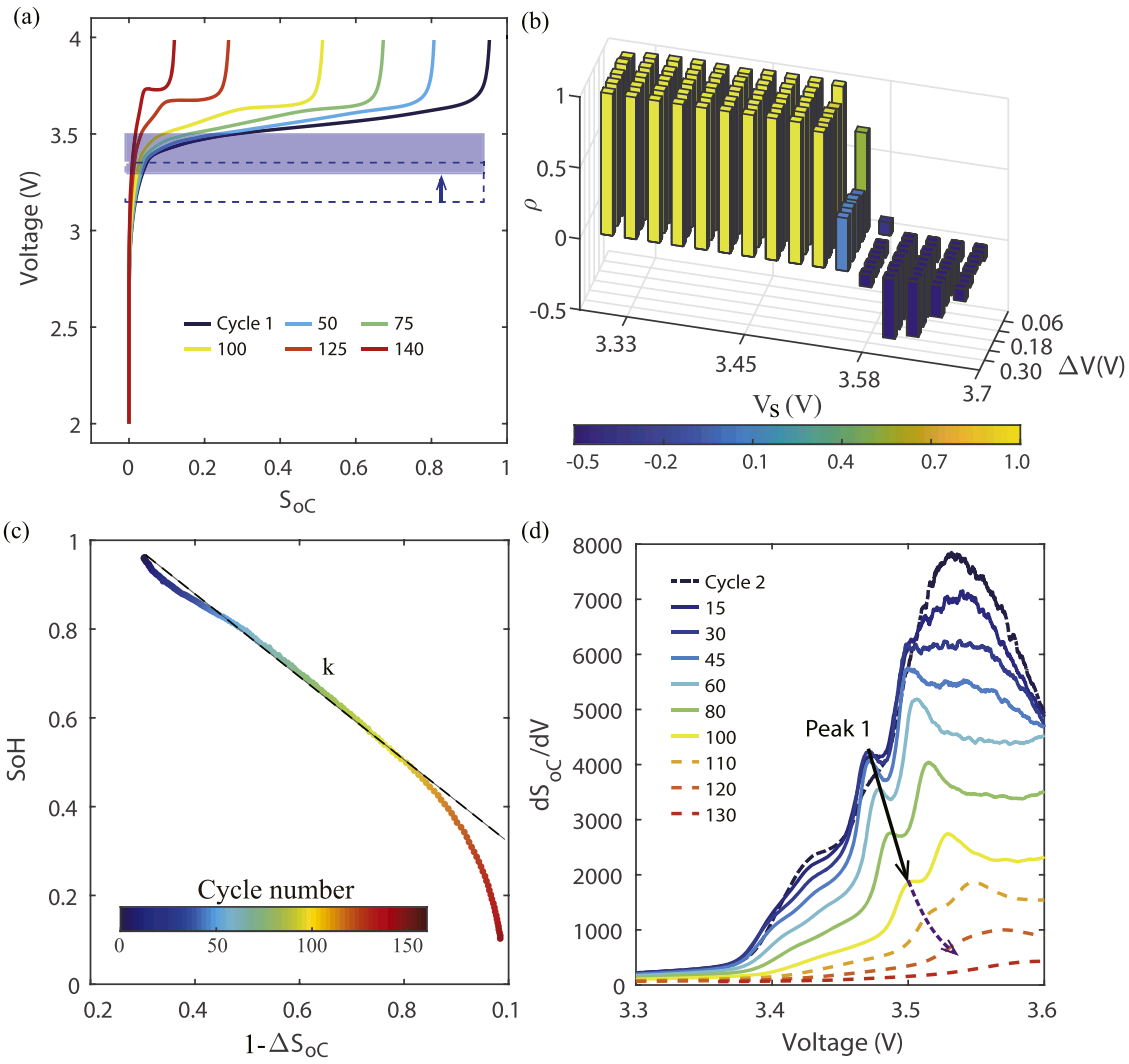

Fig. 3. The S_{oH}-ΔS_{oC} evolution rule at the charge stage in the total life cycle of the batteries, cycled with CC—CV mode (2.5C-3.0D). (a) The voltage-S_{oC} evolution curve during the 2.5C CC charge stages at different indicated cycles; (b) The spearman correlation coefficient image between SoH and ΔS_{oC} with different $(\Delta V, V_s)$ conditions; (c) The SoH-$(1-\Delta S_{oC})$ correlation plot with the voltage window $(\Delta V = 0.3, V_s = 3.3)$; (d) The dS_{oc}/dV-voltage curves at different cycles.

and V_s. As seen from Fig. 2a, for each V_s and ΔV, the ΔS_{oC} can be read at the voltage $(\Delta V,\ V_s)$. We have $S_{oH,j}$ and $\Delta S_{oC,j}$ from a voltage-time curve at the j-th cycle. After converting $(\Delta S_{oC,j})$ and $(S_{oH,j})$ to ranks $\mathrm{R}(\Delta S_{oC,j})$ and $\mathrm{R}(S_{oH,j})$, we define d_j the difference between the two ranks, $d_j = R(\Delta S_{oC,j}) - R(S_{oH,j})$. The Spearman correlation coefficient ρ can be computed using the formula below

$$\rho = 1 - \frac{6\sum_{j=1}^{n}(d_j)^2}{n(n^2-1)}, \tag{1}$$

where n is the total number of cycles, which is battery-specific. Note that ρ ranges from -1 to 1, where $\rho = 1$, 0, and -1 indicate a perfect positive association of ranks, no association of ranks, and a perfect negative association between ranks, respectively.

The correlation between SoH and ΔS_{oC}, with different voltage windows $(\Delta V, V_s)$ from the voltage-(1-S_{oC}) curve at the 3C CC discharge rate, is then examined. As seen in Fig. 2b, a strong positive association between SoH and ΔS_{oC} is found at the initial discharging process (3.2 to 2.9 V). As the selected voltage window slides down to lower voltages, the correlation reduces and disappears (ρ becomes negative as the voltage drops from 2.9 to 2.5 V). Taking the sliding voltage window $\Delta V = 0.3, V_s = 3.3$ as an example, see the S_{oH}-$(1-\Delta S_{oC})$ curve in Fig. 2c, a strong correlation is indicated between SoH and ΔS_{oC}: SoH firstly decreases proportionally with decreasing ΔS_{oC} at the initial degradation stage, and then followed by a nonlinear degradation as ΔS_{oC} reduces further.

The incremental capacity (IC) curve, calculated as the derivative of S_{oC} with respect to voltage (dS_{oC}/dV vs. V), is commonly applied to reveal characteristic peaks associated with different chemical reaction processes. The peak features in IC curves, including the amplitude, area, and peak shifts, may change with battery cycling, which can be applied for SoH analyses [49]. Fig. 2d shows the IC curves at different cycles extracted from the tested voltage vs. (1-S_{oC}) curves (Fig. 2a). Often there are two peaks on the IC curves at an early degradation stage (marked by the solid black arrow in Fig. 2d), and the intensity of the two peaks decay with cycling. At this stage, there is a strong linear correlation between SoH and $1-\Delta S_{oC}$, as demonstrated in Fig. 2c. Further cycling leads to accelerated degradation, as exemplified by the significant intensity decay and position offset of Peak 1 to the lower end voltage (marked by the dashed black arrow in Fig. 2d). Peak 2 becomes invisible at this stage. The accelerated degradation regime on IC curves in Fig. 2d refers perfectly to the nonlinear SoH-ΔS_{oC} evolution period shown in Fig. 2c.

3.2. S_{oH}-ΔS_{oC} evolution during charging

The S_{oH}-ΔS_{oC} correlation is also present at the CC charge stages, as

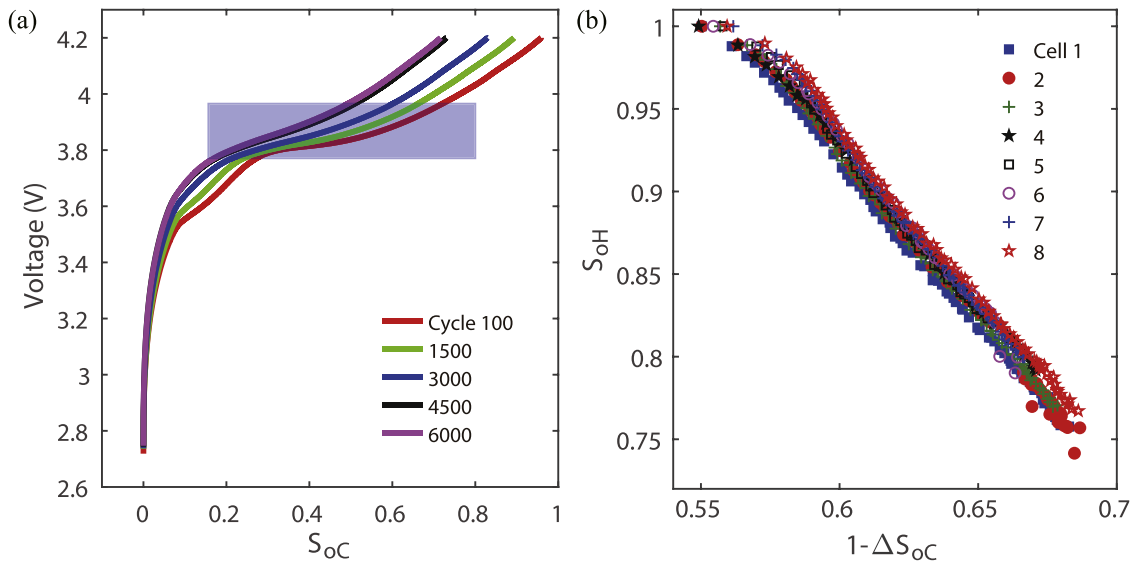

Fig. 4. Validation of the S_{oH}-ΔS_{oC} model during CC charging by the pouch LIBs. The exploited dataset includes eight Kokam pouch batteries from Birkl et al. [59, 60]. (a) The voltage-S_{oC} evolution curves during the 1C CC charge stages at different cycles; (b) The SoH-(1-ΔS_{oC}) relationship with the sliding voltage window ($\Delta V = 0.2, V_s = 3.8$) at the 1C charge rate. .

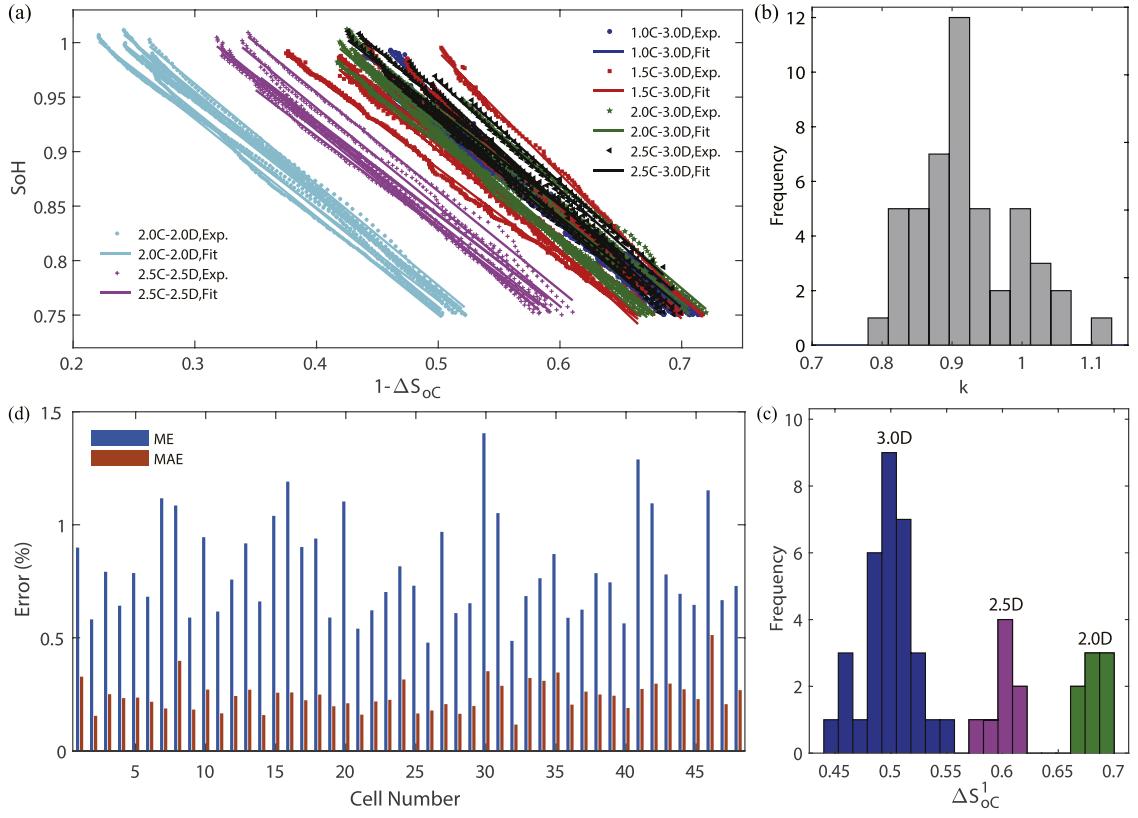

Fig. 5. The linear S_{oH}-ΔS_{oC} evolution. (a) The linear S_{oH}-ΔS_{oC} evolution of LIBs with different CC charge and CC discharge rates (Markers: experimental results; Solid lines: fitting results). Distributions of (b) k and (c) ΔS^1_{oC} from linear fitting results. (d) The fitting errors of each battery in a dataset of 48 batteries are examined.

shown in Fig. 3. By choosing a voltage window (the light blue color marked region in Fig. 3a) and sliding along the voltage-time curves from low voltage to high voltage, we show in Fig. 3b the Spearman coefficient ρ between SoH with ΔS_{oc}. A strong correlation is indicated at the initial charge stage with low voltages. Fig. 3c shows the S_{oH}-ΔS_{oC} relationship with a suitable voltage window of $\Delta V = 0.3, V_s = 3.3$, a linear evolution is observed for SoH to 0.5. In the linear S_{oH}-ΔS_{oc} evolution stage, Peak 1 shows an intensity reduction and position offset to the higher voltage end (marked by the solid black arrow in Fig. 3d). Progressive decay in SoH, as seen in Fig. 3c, may be identified by the leveled-out intensity Peak 1, as indicated by the dashed blue arrow in Fig. 3d.

Our sliding voltage window method is further validated with another experimental dataset of 8 Kokam pouch batteries (SLPB 533459H, 0.74Ah nominal capacity) with a mixed positive electrode of lithium

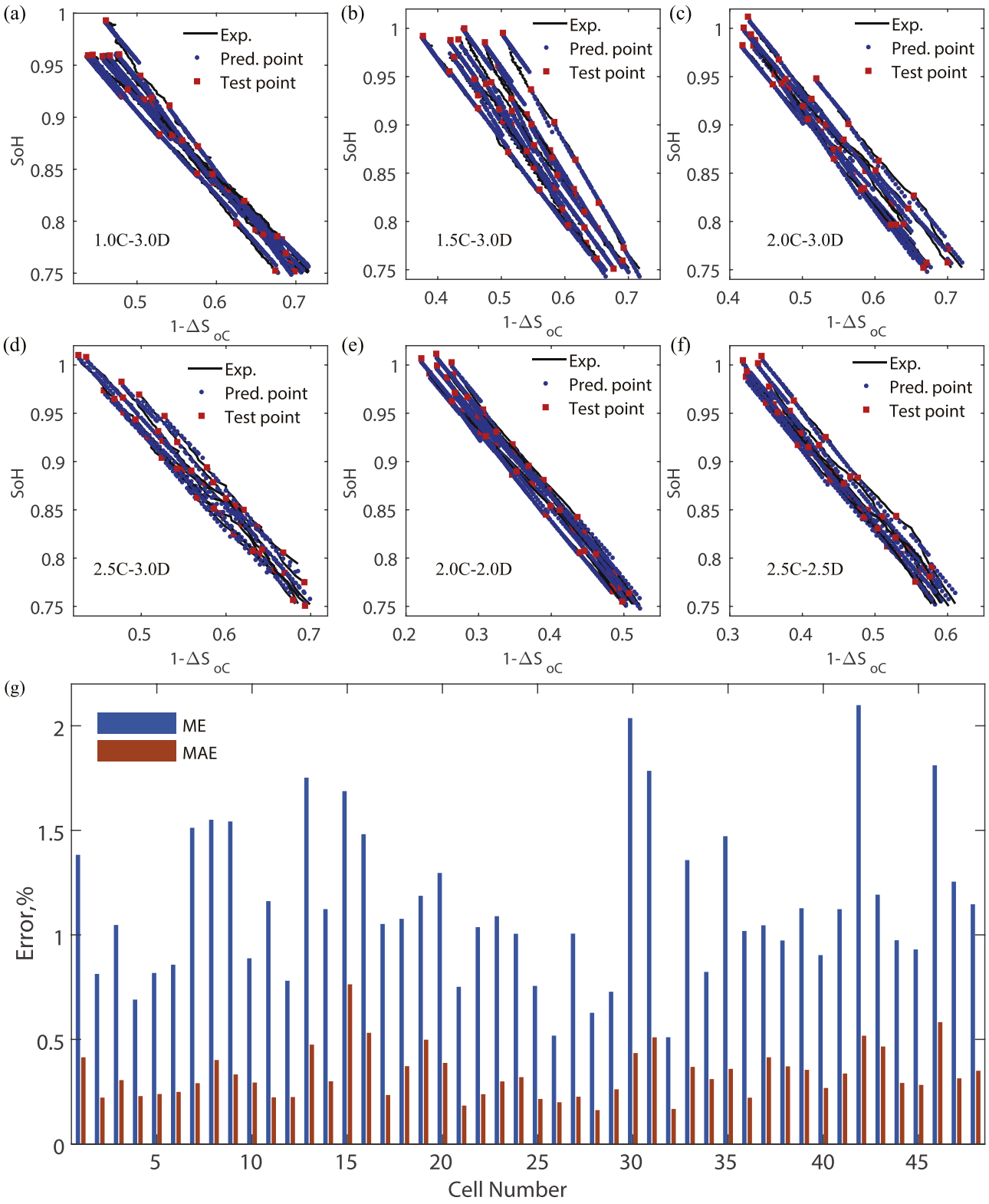

Fig. 6. Application by utilizing the linearity of S_{oH}-ΔS_{oC} for SoH prediction. (a-f) The linear S_{oH}-ΔS_{oC} evolution of LIBs with different charge and discharge rates (blue points: predicted SoH evolution; black solid lines: experimental results; red points: certain test points from experiments). (g) The errors of our prediction errors for the 48 batteries.

cobalt oxide and lithium nickel cobalt oxide, and graphite as negative electrode material [59,60]. The pouch batteries were cycled with two different types of charge and discharge profiles (the dynamic-driving-profile and the characterization cycles) at 40 C^{o}. The dynamic-driving-profile is composed of a 2C (1C corresponds to 0.74 A) CC charge and the Artemis urban drive cycle with an average discharge current of 1.36 A [61]. After each 100 dynamic-driving-profile cycles, a characterization cycle is then employed with the 1C CC charge and discharge. Fig. 4a shows the voltage-S_{oC} curves during charging at different characterization cycles. For the S_{oH}-(1-ΔS_{oC}) correlation

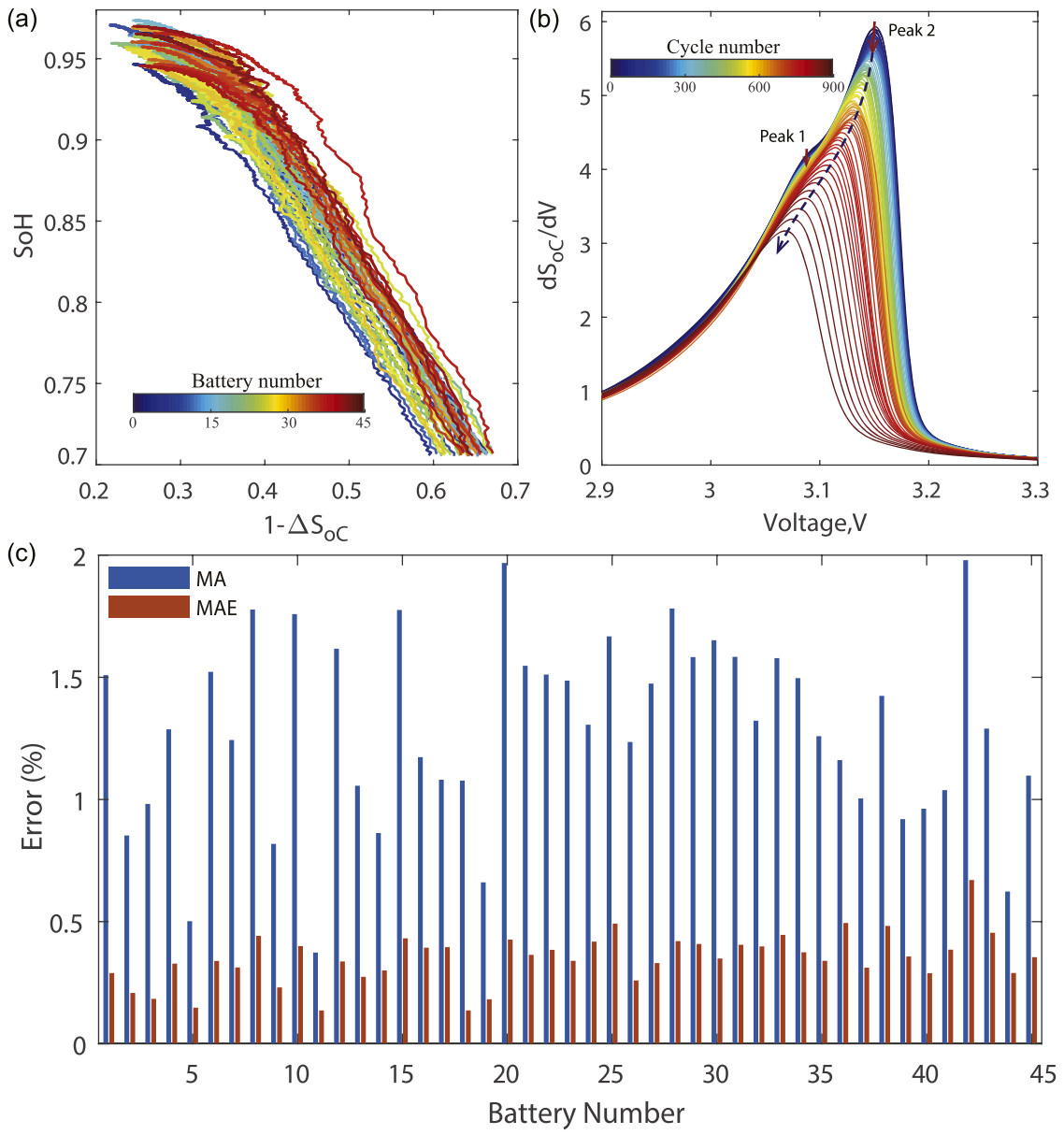

Fig. 7. Validation of the S_{oH}-ΔS_{oC} linearity from the 4C CC discharge stages in a dataset including 45 A123 LFP/graphite batteries from Attia *et al.* [63]. (a) The S_{oH}-(1-ΔS_{oC}) plots with the voltage window ($\Delta V = 0.3, V_s = 3.3$). (b) The d$S_{oC}$/d$V$-voltage curves at different cycles from one battery of the indicated dataset. (c) The fitting error on SoH of each battery in comparison with the extracted one from the linear SoH-ΔS_{oC} relationship.

evaluation, a voltage window ($\Delta V = 0.2, V_s = 3.8$), in the 1C CC charge stage (light blue color marked region in Fig. 4a), is employed. We show in Fig. 4b the S_{oH}-(1-ΔS_{oC}) evolution curves of the 8 Kokam batteries. The S_{oH}-(1-ΔS_{oC}) evolution pattern is in concerted with what we demonstrated in Figs. 2c and 3c.

3.3. Linear S_{oH}-ΔS_{oC} relationship

A total of 48 LISHEN LFP/graphite LIBs with 6 different charge-discharge rates are then employed for cycling performance check. The linear evolution stage of the S_{oH}-ΔS_{oC} relationship is then extracted from voltage-time curves at CC discharge stages. The cut-off condition of the linear S_{oH}-ΔS_{oC} evolution rule is set to an offset voltage of Peak 1 of 0.3% in IC curves, deviating from the initial voltage position. The extracted linear S_{oH}-ΔS_{oC} evolution stage of the total 48 batteries falls primarily within the region S_{oH}>0.75 (Fig. 5a), which is the typical working condition as the first-life of LIBs with high reliability [62]. We then define the linear S_{oH}-ΔS_{oC} relationship as

$$S_{oH} = 1 + k\left(\Delta S_{oC} - \Delta S_{oC}^{1}\right), \tag{2}$$

where k reflects the degradation slope and ΔS_{oC}^{1} is the extrapolated interception at $S_{oH} = 1$.

The S_{oH}-ΔS_{oC} curves from a broad variety of charging rates, as seen in Fig. 5a, suggest the robustness of the linear degradation characterized by k and ΔS_{oC}^{1}. The histograms of k and ΔS_{oC}^{1} are shown in Fig. 5b and Fig. 5c, respectively. It can be seen that the slope k is insensitive to the CC charge and CC discharge rates, at least within our exploration with 48 cells. The trend of ΔS_{oC}^{1} is evident, it increases as decreasing discharge rate, as shown in Fig. 5c.

The linearity of S_{oH}-ΔS_{oC} is crucial to the SoH estimation. We now demonstrate that this feature can be utilized to assess SoH by adopting shallow (dis)charging. We define both commonly used error criteria to evaluate the linearity as the Maximum Error (ME), ME $= \underset{i=1,2,\ldots,n}{max}\left(y_i - \widehat{y}_i\right)$ and the Mean Absolute Error (MAE), MAE $= \frac{1}{n}\sum_{i=1}^{n}\left|y_i - \widehat{y}_i\right|$. Here y_i and

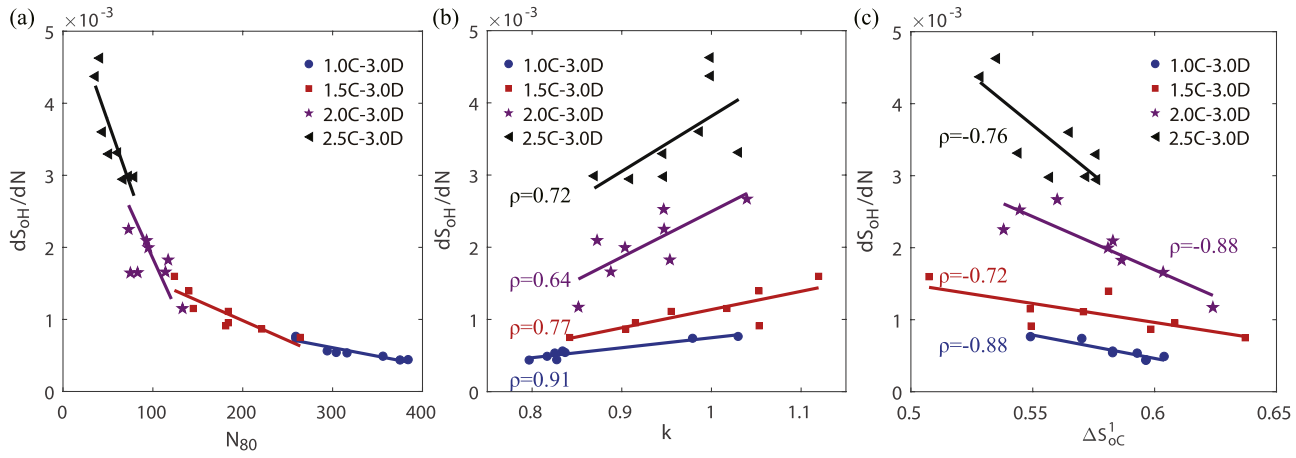

Fig. 8. The correlation analyses between linear S_{oH}-ΔS_{oC} evolution performance and cycle-life of the 32 LISHEN LFP/graphite batteries. (a) The dS_{oH}/dN-N_{80} (N_{80}: total cycle number till SoH descending to 0.8), (b) dS_{oH}/dN-k and (c) dS_{oH}/dN-ΔS^1_{oC} plots under charge rates 1.0C, 1.5C, 2.0C, and 2.5C, but the same 3C discharge rate. (Symbols: experimental data; Solid lines: linear fitting).

$\hat{y}_i$ are observed and fitted SoH, respectively, and n is the total number of the tested SoH. The fitting errors of 48 batteries are shown in Fig. 5d. We can see that the fitted MEs of SoH range from 0.4% to 1.4% in the 48 batteries, and the MAEs are smaller by 0.5%.

We then predicted the SoH evolution of the 48 batteries based on k and ΔS^1_{oC}. Fig. 6a-f show the comparison between experimentally measured (black solid lines) and predicted SoH (blue points). For the SoH prediction, accompanied with a drop of SoH up to 0.04 (red points), the k value was then corrected once to improve accuracy. In engineering practice, for example in electrical vehicles, the parameter correction process can be performed during the annual maintenance of vehicles. The predictability of our model for the 48 batteries is shown in Fig. 6g. We can see that the ME of SoH ranges from 0.5% to 2% in the 48 batteries, and the MAE is within 0.7%, which are comparable to fitting results shown in Fig. 5d. The efficacy of the model demonstrated through Fig. 6 highlights the robust predictability when employing the linear S_{oH}-ΔS_{oC} relationship for SoH estimation.

We further validated the S_{oH}-ΔS_{oC} linearity by another dataset of a total 45 LIBs [63] with the LFP cathode and the graphite anode (A123, 1.1Ah nominal capacity). The 45 A123 LIBs were cycled with the same discharging profiles using 4C (1C=1.1A) CC discharge rate till 2 V CV mode with a 1/50C cut-off current. We show in Fig. 7 the S_{oH}-ΔS_{oC} evolution by applying the voltage window ($\Delta V = 0.3, V_s = 3.3$) to the 4C discharge voltage-time curve. A strong correlation between SoH and ΔS_{oC} can also be found in Fig. 7a. Different from the S_{oH}-ΔS_{oC} relationship shown in Fig. 2c (LISHEN LFP/graphite batteries), a nonlinear evolution occurs in the initial stage, predominantly when SoH>0.93, and followed by a linear evolution until SoH=0.7. Two different evolution stages from the IC curves are shown in Fig. 7b: for the two peaks shown in the IC curves, and the intensity of peak 1 reduces at the initial nonlinear stage and disappears by the end. In contrast, the magnitude of Peak 2 drops proportionally with cycling in the linear SoH-ΔS_{oC} region. The linearity of the evolution stage is then examined for each battery in the dataset composing 45 A123 batteries (Fig. 7c). The fitted ME of SoH ranges from 0.4% to 2.0%, and the MAE is smaller by 0.5%. The ME, based on SoH measured against SOH predicted, ranges from 0.4% to 2% in the 48 batteries, and the MAE is even smaller and within 0.7%. In comparison with the error results from other SoH estimation models [25], the proposed model can give more competitive SoH estimation on accuracy. Applications of our model to data from two independent studies (Figs. 5 and 7) indicate its efficiency and capability for generalization.

4. Cycle-life property evaluated by the linear S_{oH}-ΔS_{oc} indexes

We analyze the correlation between the linear S_{oH}-ΔS_{oC} evolution and the cycle life of batteries. A total of 32 LISEHN LFP/graphite batteries with the same 3C discharge rate (constant current) and four different charge rates (Groups 1 to 4 described in Table 1) are employed to extract the linear S_{oH}-ΔS_{oC} evolution (see Fig. 5a). The average degradation rate of SoH, defined by dS_{oH}/dN, may then serve the purpose of indicating cycle-life property of LIBs. Since the linear SoH-ΔS_{oC} evolution of LIBs is within their serving status of high reliability, e.g., for electric vehicle batteries, SoH>0.8, we show in Fig. 8a the correlation between dS_{oH}/dN and the cycle-life N_{80} – the cycle number till SoH degrades to 0.8. The tight negative correlation between dS_{oH}/dN and N_{80} indicates that the batteries with the lower dS_{oH}/dN would exhibit better cycle-life properties.

The correlations of dS_{oH}/dN with k and ΔS^1_{oC} are shown in Fig. 8b and 8c, respectively. The dS_{oH}/dN vs. k plots, shown in Fig. 8b, indicate positive correlation for the same (dis)charging profile. In particular, the strongest positive correlation between dS_{oH}/dN and k in Fig. 8b occurs when 1.0C charge rate was applied, where its degradation rate of SoH is the lowest among the four (dis)charging profiles investigated here. We then check the correlation between dS_{oH}/dN and the extrapolated interception ΔS^1_{oC}. The correlation between dS_{oH}/dN and ΔS^1_{oC} is shown in Fig. 8c, indicating a negative correlation. Results shown in Fig. 8 then suggest that the batteries with lower k and greater ΔS^1_{oC} would have better cycling performance. As a corollary, both k and ΔS^1_{oC} may be adopted as auxiliary parameters, in addition to S_{oH}, to further differentiate the remaining life of batteries with close SoH.

5. Conclusion

Through experimental investigations and theoretical analyses by taking a sliding voltage window in the constant-current (dis)charge voltage-time curve of LIBs, we explored the correlation between SoH and the incremental SoC (ΔS_{oC}): In commonly reliable SoH operation, the ΔS_{oC} and the SoH follow a linear relationship within a suitable voltage region. The linearity of S_{oH}-ΔS_{oC} is also validated through experiments with different battery types and manufacturers, and source data from different groups. Such a linearity between S_{oH}-ΔS_{oC}, as characterized by two core indexes (the slope k and the extrapolated interception ΔS^1_{oC}), can then be employed to estimate the SoH of LIBs during onward cycling, by adopting shallow (dis)charge.

By virtue of the linearity between S_{oH}-ΔS_{oC}, we may acquire sequential evaluation for SoH of LIBs in onward cycling by adopting

shallow (dis)charge. In comparison with existing proposals to characterize SoH of LIBs [23–27], we find the following features makes this proposal a distinct one: (1) Our strategy of estimating SoH is applicable to both the commonly applied CC charge and CC discharge profiles in engineering, with no restriction to (dis)charging rates; (2) The method is simple and easy to be implemented since the input is voltage – time curve at even shallow (dis)charging; (3) The method is robust in terms of efficacy and accuracy for SoH evaluation regardless of the quality of voltage – time curve, which makes the method fit to quick assessment, in less than a few minutes.

In conclusion, we report in this paper a practicable SoH estimation model for LIBs, which after the initial two to three full cycles of charge-discharge, we may evaluate with high fidelity the SoH based on partial charge and discharge segment method. The proposed SoH estimation is quick and non-destructive, and could be applied to monitor the health of commercial LIBs in service.

Credit author statement

Y. Wei conceived the project; J. Wen and Q. Zou did the data analysis; C. Chen performed the experiments. All authors involved in paper writing, data analysis and discussion.

Declaration of Competing Interest

The authors declare that they have no known competing financial interests or personal relationships that could have appeared to influence the work reported in this paper.

Data availability

Data will be made available on request.

Acknowledgments

Y. Wei acknowledges support from the National Natural Science Foundation of China (NSFC) Basic Science Center for 'Multiscale Problems in Nonlinear Mechanics' (No. 11988102), and J. Wen thanks support from NSFC (No. 12002343). C. Chen would like to thank the Institute of Mechanics, Chinese Academy of Sciences for the financial support given for this work (No. E1Z1010901).

References

[1] M. Armand, J.M. Tarascon, Building better batteries, Nature 451 (2008) 652–657, https://doi.org/10.1038/451652a.
[2] M. Yoshio, R.J. Brodd, A. Kozawa, Lithium-ion Batteries, 1, Springer, New York, 2009, pp. 2–3.
[3] B. Dunn, H. Kamath, J.M. Tarascon, Electrical energy storage for the grid: a battery of choices, Science 334 (2011) 928–935, https://doi.org/10.1126/science.1212741.
[4] S.K. Jung, H. Gwon, J. Hong, K.Y. Park, D.H. Seo, H. Kim, J. Hyun, W. Yang, K. Kang, Understanding the degradation mechanisms of LiNi0.5Co0.2Mn0.3O2 cathode material in lithium ion batteries, Adv. Energy Mater. 4 (2014), 1300787, https://doi.org/10.1002/aenm.201300787.
[5] S.M. Rezvanizaniani, Z. Liu, Y. Chen, J. Lee, Review and recent advances in battery health monitoring and prognostics technologies for electric vehicle (EV) safety and mobility, J. Power Sources 256 (2014) 110–124, https://doi.org/10.1016/j.jpowsour.2014.01.085.
[6] G.W. You, S. Park, D. Oh, Diagnosis of electric vehicle batteries using recurrent neural networks, IEEE Trans. Ind. Electron. 64 (2017) 4885–4893, https://doi.org/10.1109/TIE.2017.2674593.
[7] S. Son, S. Jeong, E. Kwak, J.H. Kim, K.Y. Oh, Integrated framework for SOH estimation of lithium-ion batteries using multiphysics features, Energy 238 (2022), 121712, https://doi.org/10.1016/j.energy.2021.121712.
[8] G. Vennam, A. Sahoo, S. Ahmed, A survey on lithium-ion battery internal and external degradation modeling and state of health estimation, J. Energy Storage 52 (2022), 104720, https://doi.org/10.1016/j.est.2022.104720.
[9] F. Huet, A review of impedance measurements for determination of the state-of-charge or state-of-health of secondary batteries, J. Power Sources 70 (1998) 59–69, https://doi.org/10.1016/S0378-7753(97)02665-7.
[10] L. Lu, X. Han, J. Li, J. Hua, M. Ouyang, A review on the key issues for lithium-ion battery management in electric vehicles, J. Power Sources 226 (2013) 272–288, https://doi.org/10.1016/j.jpowsour.2012.10.060.
[11] X. Hu, F. Feng, K. Liu, L. Zhang, J. Xie, B. Liu, State estimation for advanced battery management: key challenges and future trends, Renew. Sustain. Energy Rev. 114 (2019), 109334, https://doi.org/10.1016/j.rser.2019.109334.
[12] M. Broussely, P. Biensan, F. Bonhomme, P. Blanchard, S. Herreyre, K.R.J. Nechev, Staniewicz, Main aging mechanisms in Li ion batteries, J. Power Sources 146 (2005) 90–96, https://doi.org/10.1016/j.jpowsour.2005.03.172.
[13] M.B. Pinson, M.Z. Bazant, Theory of SEI formation in rechargeable batteries: capacity fade, accelerated aging and lifetime prediction, J. Electrochem. Soc. 160 (2012) A243, https://doi.org/10.1149/2.044302jes.
[14] J. Wen, Y. Wei, Y.T. Cheng, Stress evolution in elastic-plastic electrodes during electrochemical processes: a numerical method and its applications, J. Mech. Phys. Solids 116 (2018) 403–415, https://doi.org/10.1016/j.jmps.2018.04.006.
[15] C. Wang, J. Wen, F. Luo, B. Quan, H. Li, Y. Wei, C. Gu, J. Li, Anisotropic expansion and size-dependent fracture of silicon nanotubes during lithiation, J. Mater. Chem. 7 (2019) 15113–15122, https://doi.org/10.1039/C9TA00519F.
[16] K.J. Park, J.Y. Hwang, H.H. Ryu, F. Maglia, S.J. Kim, P. Lamp, C.S. Yoon, Y.K. Sun, Degradation mechanism of Ni-enriched NCA cathode for lithium batteries: are microcracks really critical? ACS Energy Lett. 4 (2019) 1394–1400, https://doi.org/10.1021/acsenergylett.9b00733.
[17] C. Chen, T. Zhou, D.L. Danilov, L. Gao, S. Benning, N. Schön, R.A. Eichel, P. H. Notten, Impact of dual-layer solid-electrolyte interphase inhomogeneities on early-stage defect formation in Si electrodes, Nat. Commun. 11 (2020) 3283, https://doi.org/10.1038/s41467-020-17104-9.
[18] D. Li, Y. Wang, J. Hu, B. Lu, Y.T. Cheng, J. Zhang, *In situ* measurement of mechanical property and stress evolution in a composite silicon electrode, J. Power Sources 366 (2017) 80–85, https://doi.org/10.1016/j.jpowsour.2017.09.004.
[19] D. Bistri, C.V. Di Leo, Modeling of chemo-mechanical multi-particle interactions in composite electrodes for liquid and solid-state Li-ion batteries, J. Electrochem. Soc. 168 (2021), 030515, https://doi.org/10.1149/1945-7111/abe8ea.
[20] C. Chen, M. Jiang, T. Zhou, L. Raijmakers, E. Vezhlev, B. Wu, T.U. Schulli, D. L. Danilov, Y.J. Wei, R.A. Eichel, P.H. Notten, Interface aspects in all-solid-state Li-based batteries reviewed, Adv. Energy Mater. 11 (2021), 2003939, https://doi.org/10.1002/aenm.202003939.
[21] J. Wen, Q. Zou, Y. Wei, Physics-driven machine learning model on temperature and time-dependent deformation in lithium metal and its finite element implementation, J. Mech. Phys. Solids 153 (2021), 104481, https://doi.org/10.1016/j.jmps.2021.104481.
[22] M. Magri, B. Boz, L. Cabras, A. Salvadori, Quantitative investigation of the influence of electrode morphology in the electro-chemo-mechanical response of li-ion batteries, Electrochim. Acta 405 (2022), 139778, https://doi.org/10.1016/j.electacta.2021.139778.
[23] Z. Cui, C. Wang, X. Gao, S. Tian, State of health estimation for lithium-ion battery based on the coupling-loop nonlinear autoregressive with exogenous inputs neural network, Electrochim. Acta 393 (2021), 139047, https://doi.org/10.1016/j.electacta.2021.139047.
[24] R. Xiong, L. Li, J. Tian, Towards a smarter battery management system: a critical review on battery state of health monitoring methods, J. Power Sources 405 (2018) 18–29, https://doi.org/10.1016/j.jpowsour.2018.10.019.
[25] Y. Wang, J. Tian, Z. Sun, L. Wang, R. Xu, M. Li, Z. Chen, A comprehensive review of battery modeling and state estimation approaches for advanced battery management systems, Renew. Sustain. Energy Rev. 131 (2020), 110015, https://doi.org/10.1016/j.rser.2020.110015.
[26] S.K. Pradhan, B. Chakraborty, Battery management strategies: an essential review for battery state of health monitoring techniques, J. Energy Storage 51 (2022), 104427, https://doi.org/10.1016/j.est.2022.104427.
[27] Y.F. Guo, K. Huang, X.Y. Hu, A state-of-health estimation method of lithium-ion batteries based on multi-feature extracted from constant current charging curve, J. Energy Storage 36 (2021), 102372, https://doi.org/10.1016/j.est.2021.102372.
[28] K.S. Ng, C.S. Moo, Y.P. Chen, Y.C. Hsieh, Enhanced coulomb counting method for estimating state-of-charge and state-of-health of lithium-ion batteries, Appl. Energy 86 (2009) 1506–1511, https://doi.org/10.1016/j.apenergy.2008.11.021.
[29] D. Li, D. Yang, L. Li, L. Wang, K. Wang, Electrochemical impedance spectroscopy based on the state of health estimation for lithium-ion batteries, Energies 15 (2022) 6665, https://doi.org/10.3390/en15186665.
[30] A. Romero-Becerril, L. Alvarez-Icaza, Comparison of discretization methods applied to the single-particle model of lithium-ion batteries, J. Power Sources 196 (2011) 10267–10279, https://doi.org/10.1016/j.jpowsour.2011.06.091.
[31] M. Safari, M. Morcrette, A. Teyssot, C. Delacourt, Multimodal physics-based aging model for life prediction of Li-ion batteries, J. Electrochem. Soc. 156 (2008) A145, https://doi.org/10.1149/1.3043429.
[32] X. Han, M. Ouyang, L. Lu, J. Li, Simplification of physics-based electrochemical model for lithium ion battery on electric vehicle. Part I: diffusion simplification and single particle model, J. Power Sources 278 (2015) 802–813, https://doi.org/10.1016/j.jpowsour.2014.12.101.
[33] J. Wen, Q. Zou, Z. Zhang, J. Shi, Y. Wei, The scaling of charging rate and cycle number of commercial batteries, Acta Mech. Sin. 38 (2022) 1–10, https://doi.org/10.1007/s10409-022-22108-x.
[34] A. Farmann, D.U. Sauer, A comprehensive review of on-board State-of-Available-Power prediction techniques for lithium-ion batteries in electric vehicles, J. Power Sources 329 (2016) 123–137, https://doi.org/10.1016/j.jpowsour.2016.08.031.
[35] A. Eddahech, O. Briat, J.M. Vinassa, Determination of lithium-ion battery state-of-health based on constant-voltage charge phase, J. Power Sources 258 (2014) 218–227, https://doi.org/10.1016/j.jpowsour.2014.02.020.

[36] C. Liu, D. Li, L. Wang, L. Li, K. Wang, Strong robustness and high accuracy in predicting remaining useful life of supercapacitors, APL Mater. 10 (2022), 061106, https://doi.org/10.1063/5.0092074.
[37] D. Roman, S. Saxena, V. Robu, M. Pecht, D. Flynn, Machine learning pipeline for battery state-of-health estimation, Nat. Mach. Intell. 3 (2021) 447–456, https://doi.org/10.1038/s42256-021-00312-3.
[38] S. Shen, M. Sadoughi, M. Li, Z. Wang, C. Hu, Deep convolutional neural networks with ensemble learning and transfer learning for capacity estimation of lithium-ion batteries, Appl. Energy 260 (2020), 114296, https://doi.org/10.1016/j.apenergy.2019.114296.
[39] P. Guo, Z. Cheng, L. Yang, A data-driven remaining capacity estimation approach for lithium-ion batteries based on charging health feature extraction, J. Power Sources 412 (2019) 442–450, https://doi.org/10.1016/j.jpowsour.2018.11.072.
[40] K.A. Severson, P.M. Attia, N. Jin, N. Perkins, B. Jiang, Z. Yang, M.H. Chen, M. Aykol, P.K. Herring, D. Fraggedakis, M.Z. Bazant, S.J. Harris, W.C. Chueh, R. D. Braatz, Data-driven prediction of battery cycle life before capacity degradation, Nat. Energy 4 (2019) 383–391, https://doi.org/10.1038/s41560-019-0356-8.
[41] E. Chemali, P.J. Kollmeyer, M. Preindl, Y. Fahmy, A. Emadi, A convolutional neural network approach for estimation of Li-ion battery state of health from charge profiles, Energies 15 (2022) 1185, https://doi.org/10.3390/en15031185.
[42] Y. Fan, F. Xiao, C. Li, G. Yang, X. Tang, A novel deep learning framework for state of health estimation of lithium-ion battery, J. Energy Storage 32 (2020), 101741, https://doi.org/10.1016/j.est.2020.101741.
[43] C. Weng, Y. Cui, J. Sun, H. Peng, On-board state of health monitoring of lithium-ion batteries using incremental capacity analysis with support vector regression, J. Power Sources 235 (2013) 36–44, https://doi.org/10.1016/j.jpowsour.2013.02.012.
[44] J. Cannarella, C.B. Arnold, State of health and charge measurements in lithium-ion batteries using mechanical stress, J. Power Sources 269 (2014) 7–14, https://doi.org/10.1016/j.jpowsour.2014.07.003.
[45] M. Berecibar, M. Garmendia, I. Gandiaga, J. Crego, I. Villarreal, State of health estimation algorithm of LiFePO4 battery packs based on differential voltage curves for battery management system application, Energy 103 (2016) 784–796, https://doi.org/10.1016/j.energy.2016.02.163.
[46] D. Yang, X. Zhang, R. Pan, Y. Wang, Z. Chen, A novel Gaussian process regression model for state-of-health estimation of lithium-ion battery using charging curve, J. Power Sources 384 (2018) 387–395, https://doi.org/10.1016/j.jpowsour.2018.03.015.
[47] Y. Deng, H. Ying, E. Jiaqiang, H. Zhou, K. Wei, J. Chen, F. Zhang, G. Liao, Feature parameter extraction and intelligent estimation of the State-of-Health of lithium-ion batteries, Energy 176 (2019) 91–102, https://doi.org/10.1016/j.energy.2019.03.177.
[48] X. Tang, C. Zou, K. Yao, K. Yao, G. Chen, B. Liu, Z. He, F. Gao, A fast estimation algorithm for lithium-ion battery state of health, J. Power Sources 396 (2018) 453–458, https://doi.org/10.1016/j.jpowsour.2018.06.036.
[49] X. Feng, C. Weng, X. He, X. Han, L. Lu, D. Ren, M. Ouyang, Online state-of-health estimation for Li-ion battery using partial charging segment based on support vector machine, IEEE Trans. Veh. Technol. 68 (2019) 8583–8592, https://doi.org/10.1109/TVT.2019.2927120.
[50] A. Barré, B. Deguilhem, S. Grolleau, M. Gérard, F. Suard, D. Riu, A review on lithium-ion battery ageing mechanisms and estimations for automotive applications, J. Power Sources 241 (2013) 680–689, https://doi.org/10.1016/j.jpowsour.2013.05.040.
[51] L. Wang, D. Lu, Q. Liu, L. Liu, X. Zhao, State of charge estimation for LiFePO4 battery via dual extended kalman filter and charging voltage curve, Electrochim. Acta 296 (2019) 1009–1017, https://doi.org/10.1016/j.electacta.2018.11.156.
[52] P. Qin, L. Zhao, Z. Liu, State of health prediction for lithium-ion battery using a gradient boosting-based data-driven method, J. Energy Storage 47 (2022), 103644, https://doi.org/10.1016/j.est.2021.103644.
[53] D. Liu, J. Pang, J. Zhou, Y. Peng, M. Pecht, Prognostics for state of health estimation of lithium-ion batteries based on combination Gaussian process functional regression, Microelectron. Reliab. 53 (2013) 832–839, https://doi.org/10.1016/j.microrel.2013.03.010.
[54] Y. Guo, K. Huang, X. Yu, Y. Wang, State-of-health estimation for lithium-ion batteries based on historical dependency of charging data and ensemble SVR, Electrochim. Acta 428 (2022), 140940, https://doi.org/10.1016/j.electacta.2022.140940.
[55] X. Li, Z. Wang, L. Zhang, C. Zou, D.D. Dorrell, State-of-health estimation for Li-ion batteries by combing the incremental capacity analysis method with grey relational analysis, J. Power Sources 410 (2019) 106–114, https://doi.org/10.1016/j.jpowsour.2018.10.069.
[56] J. Meng, L. Cai, D.I. Stroe, X. Huang, J. Peng, T. Liu, R. Teodorescu, An automatic weak learner formulation for lithium-ion battery state of health estimation, IEEE Trans. Ind. Electron. 69 (2021) 2659–2668, https://doi.org/10.1109/TIE.2021.3065594.
[57] Y. Li, K. Li, X. Liu, Y. Wang, L. Zhang, Lithium-ion battery capacity estimation—A pruned convolutional neural network approach assisted with transfer learning, Appl. Energy 285 (2021), 116410, https://doi.org/10.1016/j.apenergy.2020.116410.
[58] E.C. Fieller, H.O. Hartley, E.S. Pearson, Tests for rank correlation coefficients. I, Biometrika 44 (1957) 470–481, https://doi.org/10.2307/2332878.
[59] C. Birkl, Diagnosis and Prognosis of Degradation in Lithium-Ion batteries, Doctoral dissertation, University of Oxford, 2017.
[60] C.R. Birkl, M.R. Roberts, E. McTurk, P.G. Bruce, D.A. Howey, Degradation diagnostics for lithium ion cells, J. Power Sources 341 (2017) 373–386, https://doi.org/10.1016/j.jpowsour.2016.12.011.
[61] M. André, The ARTEMIS European driving cycles for measuring car pollutant emissions, Sci. Total Environ. 334 (2004) 73–84, https://doi.org/10.1016/j.scitotenv.2004.04.070.
[62] P.A. Christensen, P.A. Anderson, G.D. Harper, S.M. Lambert, W. Mrozik, M. A. Rajaeifar, M.S. Wise, O. Heidrich, Risk management over the life cycle of lithium-ion batteries in electric vehicles, Renew. Sustain. Energy Rev. 148 (2021), 111240, https://doi.org/10.1016/j.rser.2021.111240.
[63] P.M. Attia, A. Grover, N. Jin, K.A. Severson, T.M. Markov, Y.H. Liao, M.H. Chen, B. Cheong, N. Perkins, Z. Yang, P.K. Herring, M. Aykol, S.J. Harris, R.D. Braatz, S. Ermon, W.C. Chueh, Closed-loop optimization of fast-charging protocols for batteries with machine learning, Nature 578 (2020) 397–402, https://doi.org/10.1038/s41586-020-1994-5.